Journal of Catalysis **184,** 213–223 (1999)
Article ID jcat.1999.2432, available online at http://www.idealibrary.com on IDEAL®

# Decomposition of Methane and Subsequent Reaction of Carbonaceous Residues over $Rh/Mo/Al_2O_3$ Catalysts

Zhuojian Wang, Colin H. Rochester, and James A. Anderson[1]

*Department of Chemistry, University of Dundee, Dundee DD1 4HN, United Kingdom*

Received October 16, 1998; revised January 11, 1999; accepted January 13, 1999

**The role of a molybdenum addition to $Rh/Al_2O_3$ catalysts has been studied in the decomposition of methane and subsequent hydrogenation reactions of the hydrocarbonaceous residues produced. Mo existed as a dispersed phase over the alumina support, which, following reduction, was present as exposed isolated $Mo^{2+}$ ions and as a surface layer on Rh particles which reduced the latter's propensity to adsorb CO. Methane underwent decomposition at 673 K to generate $C_xH$ and other hydrocarbonaceous species which blocked surface sites on $Rh/Mo/Al_2O_3$ in the order bridging sites on Rh, Rh gem-dicarbonyl, $Mo^{2+}$, and Rh on-top sites. A further proportion of the coke generated was located on the alumina support surface. Subsequent hydrogenation of the coked $Rh/Mo/Al_2O_3$ catalyst showed two maxima in product formation, the first between room temperature and 350 K and the second between 375 and 475 K, whereas methane was detected only at ca. 473 K for $Rh/Al_2O_3$ in the absence of Mo. The presence of Mo in the $Rh/Al_2O_3$ catalyst enhances the extent to which coke removal takes place in hydrogen at low temperatures, possibly by restricting the mobility, and thus the ageing, of the residues. Restructuring of the carbonaceous residues occurs in the presence of CO for $Rh/Al_2O_3$ but is less significant for $Rh/Mo/Al_2O_3$.** 

## INTRODUCTION

The conversion of methane to higher value products represents a considerable challenge to the industrial chemist and the academic community (1). In addition to the indirect routes involving the formation of syngas (2, 3), direct routes involve oxidative coupling (4) and selective oxidation to methanol and formaldehyde (5). An additional nonoxidative route via a two step process involving high temperature decomposition followed by lower temperature hydrogenation has been shown to be feasible (6). Among the Pt group metals, rhodium has been reported to be the most active in methane decomposition (7, 8) and is a plausible catalyst for higher hydrocarbon formation as the relative amounts of $\alpha$, $\beta$, and $\gamma$ carbon types can be modified by reaction conditions (6, 8, 9). Although Gutzi *et al*. indicate that one approach to modifying the relative stability (and hence reactivity and selectivity) of the $CH_x$ species is through alloying to modify the metal–carbon bond (6), the number of studies involving bimetallic rhodium-containing catalysts for this reaction is limited. The effects of alloying rhodium with copper on the decomposition of methane and subsequent hydrogenation have been reported (10, 11).

There have been numerous recent reports of the direct conversion of methane to benzene over molybdenum-based, and in particular, over Mo/ZSM-5 catalysts (12–16). One report indicates the advantages of the addition of platinum to Mo/ZSM-5 catalysts (17). In the present paper, the influence of molybdenum on the formation and hydrogenation of carbonaceous deposits on rhodium catalysts has been studied along with the use of chemisorption and FTIR of adsorbed CO to obtain information regarding the distribution, coverage, and location of these deposits.

## EXPERIMENTAL

Alumina (Degussa C, 110 $m^2 g^{-1}$) was treated with an aqueous solution of ammonium molybdate to give a loading of 10 wt% $MoO_3$, dried overnight at 383 K and then calcined in a flow of air at 773 K for 3 h. A fraction of this sample was retained for background experiments. The remainder was impregnated with an aqueous solution of rhodium nitrate to achieve a 0.5 wt% metal loading and then was dried overnight at 383 K before calcination in air at 773 K for 3 h. Hydrogen chemisorption was performed using loose powder while 25-mm diameter self-supporting disks (ca. 100 mg) were used in infrared experiments. For reaction studies, 0.15 g of sample was sieved in the 52–72 mesh range. In all cases, samples were reduced *in situ* within the respective apparatus in a flow (100 $cm^3 min^{-1}$) of hydrogen at 673 K for 2 h.

The hydrogenation of carbonaceous deposits generated by a reaction between the reduced catalyst surface and methane was studied by first exposing the catalyst at 673 K to a flow (20 $cm^3 min^{-1}$) of methane at 1 atm for 18, 30, or 40 min. The system was then flushed with nitrogen while cooling to ca. 325 K and then replacing the nitrogen with hydrogen (30 $cm^3 min^{-1}$, 1 atm) before slowly raising the

[1] To whom correspondence should be addressed.



0021-9517/99 $30.00

temperature to ca. 500 K. Analyses at increasing temperature were performed by injection from the gas stream at ca. 25 K intervals into a Perkin Elmer 8410 gas chromatograph fitted with a gas sampling valve and FID. Product separation was achieved using a 1.83-m column containing Poropak Q.

Hydrogen adsorption isotherms were measured on clean and methane-treated surfaces. The catalyst at 673 K was exposed to 100 torr $CH_4$ for 18 min and then evacuated for 10 min at 673 K prior to cooling to 298 K and exposure to $H_2$ over the range 0 to 250 torr. The amount of adsorbed hydrogen was estimated by extrapolation of the linear part of the isotherm to zero pressure.

Infrared spectra were recorded of adsorbed CO on clean, methane-treated, and methane- then hydrogen-treated surfaces. Methane-treated surfaces were prepared as for hydrogen chemisorption measurements followed by the recording of a spectrum of the sample at 298 K and exposure to CO at the same temperature over the range 0–29 torr. In the case of methane followed by hydrogen treatment, samples were exposed to 200 torr $H_2$ at 298, 373, or 473 K for 10 min followed by evacuation at the same temperature and then exposure to CO at 298 K. FTIR spectra (an average of 25 or 1000 scans for the analysis of the C–H stretching region) were recorded at 4-$cm^{-1}$ resolution using a Perkin Elmer 1720 spectrometer.

## RESULTS

Figure 1 shows the evolution of the hydrocarbon product as a function of hydrogenation temperature for samples treated for various periods of time in methane at 673 K. Figure 1A includes results from three separate experiments using fresh catalysts to illustrate the degree of reproducibility. For $Rh/Al_2O_3$, a single peak due to $CH_4$ was obtained with a maximum at 475 K, confirming previous results for methane decomposed at 623 K over $Rh/Al_2O_3$ (8). For Mo-containing samples, methane is evolved (Figs. 1A and 1B) mainly in a step below 325 K and then to a lesser extent giving a second maximum between 400 and 500 K. The profiles indicate that the hydrogenation of residues to produce methane is largely independent of the decomposition time, although there is a slight indication that the amount of residue which can be hydrogenated between 400 and 500 K is less for extended decomposition times (Fig. 1B). Extended decomposition times also resulted in a decreased yield of $C_2$ hydrocarbons (Fig. 1C), which were generated over the temperature range 325–475 K. Only in the case of intermediate coking times (30 min) did the formation of $C_2$ hydrocarbons produce a significant, well-defined maximum at 425 K.

The volumes of hydrogen taken up by the sample pre- and post-methane treatment (18 min contact) are compiled

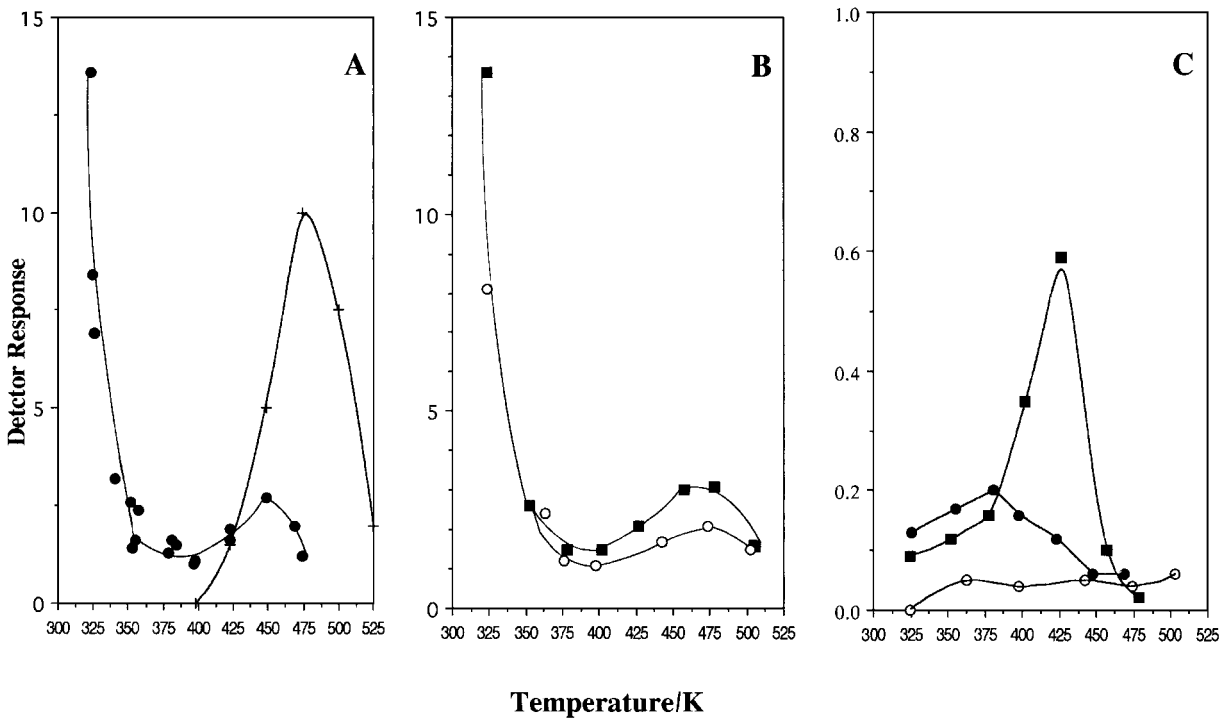


**FIG. 1.** Plots of methane (A, B) and $C_2$ (C) hydrocarbon formation as a function of hydrogenation temperature for $Rh/Mo/Al_2O_3$ previously exposed to methane at 673 K for 18 (●), 30 (■), and 40 min (○) and for $Rh/Al_2O_3$ exposed to methane at 673 K for 18 min (+).

**TABLE 1**

**Catalyst Surface Areas (BET) and Chemisorption Data before and after Methane Treatment**

| Catalyst | BET/$m^2\,g^{-1}$ | Hydrogen uptake $cm^3\,g^{-1}$ (before methane[a]) | Hydrogen uptake $cm^3\,g^{-1}$ (after methane[a]) |
|---|---|---|---|
| $Rh/Al_2O_3$ | 97 | 0.941 | 0.560 |
| $Rh/Mo/Al_2O_3$ | 96 | 0.179 | 0.067 |
| $Mo/Al_2O_3$ | 106 | — | — |
| $Al_2O_3$ | 110 | 0 | 0 |

[a] Samples exposed to 100 torr $CH_4$ for 18 min at 673 K.

in Table 1. Volumes for clean surfaces correspond with H : Rh ratios of 1.73 : 1 and 0.33 : 1 for the Mo-free and Mo-containing samples, respectively, indicating significant loss of exposed surface Rh sites by the addition of molybdenum in agreement with reports for similarly prepared $Rh/Mo/Al_2O_3$ catalysts (18). Both catalysts showed a decreased uptake after $CH_4$ treatment, with the fractional loss being greater for Mo-containing than for Mo-free samples.

Figure 2A shows the effect of decomposition time on the appearance of IR bands in the CH stretching region for $Rh/Al_2O_3$ (a–d) and $Rh/Mo/Al_2O_3$ (e). After 5 min in $CH_4$ at 673 K only a very weak broad band centred at 3045 $cm^{-1}$ was apparent although a weak maximum at 3290 $cm^{-1}$ was confirmed by exposure for longer periods of time. Exposure to $CH_4$ for 18 min led to enhanced intensity at 3045 $cm^{-1}$ and allowed bands at 3382, 3336, 3290, and 2936 to be identified (Fig. 2A(b)). Prolonged exposure for periods of up to 1 h did not lead to the appearance of additional spectral features or to significant enhancement of bands due to species detected for shorter exposure times (Fig. 2A(c,d)). Spectra of $Rh/Mo/Al_2O_3$ after 18 min coking time (Fig. 2A(e)) showed higher noise levels than the corresponding spectra for $Rh/Al_2O_3$ making any identification of bands at 3382, 3336, 3290, and 2936 impossible. However, the band at 3045 $cm^{-1}$ was readily detected with ca. twice the intensity of the corresponding band in the spectra of $Rh/Al_2O_3$.

Figure 2B shows the effect of hydrogen treatment on the species responsible for IR bands observed after methane coking on $Rh/Al_2O_3$. After exposure to hydrogen at room temperature, the 3045-$cm^{-1}$ maxima was attenuated and additional IR bands appeared at 2834 and 2948 $cm^{-1}$ (Fig. 2B(b)). Both features were enhanced by increasing the hydrogenation temperature to 373 K and an additional shoulder at 2972 $cm^{-1}$ on the latter was discernible (Fig. 2B(c)). The bands at 3382, 3336, and 3290 $cm^{-1}$ could not be clearly identified against background noise for hydrogenation temperatures of 373 K and above, although an additional band at 3191 $cm^{-1}$ became apparent in the same temperature range. A sharp band at 3015 $cm^{-1}$ became apparent in the spectra of the sample after exposure to hydrogen at 473 K (Fig. 2B(d)) and this, in addition to a similar shaped maximum at 1309 $cm^{-1}$ (not shown), indicates the formation of gaseous methane in the IR cell.

IR bands were also detected in the low frequency spectral region following methane treatment. Figure 3 shows

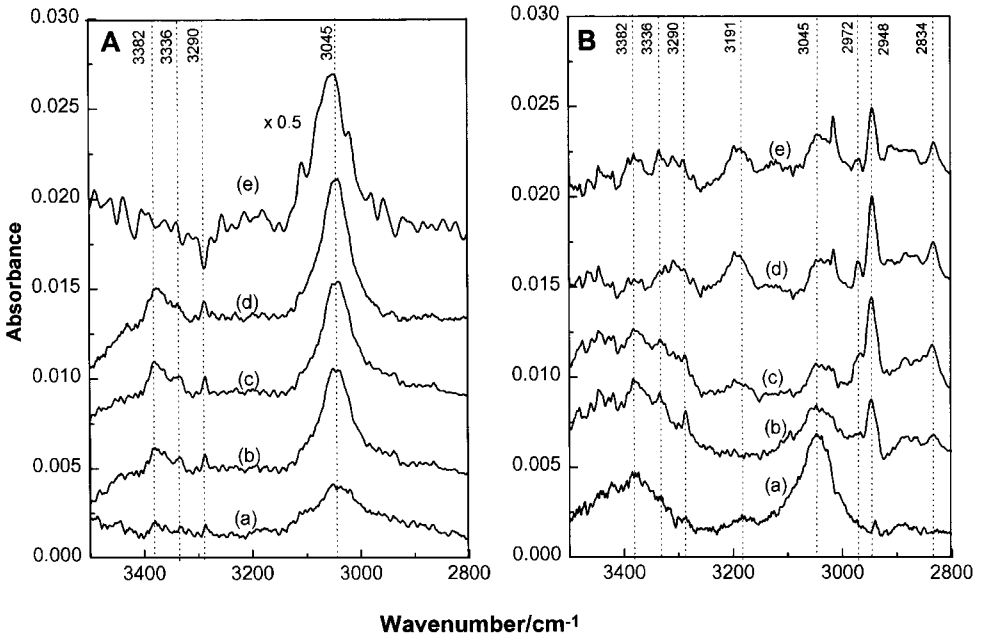


**FIG. 2.** (A) FTIR spectra of $Rh/Al_2O_3$ exposed to methane at 673 K for (a) 5, (b) 18, (c) 40, and (d) 60 min and (e) of $Rh/Mo/Al_2O_3$ exposed to methane at 673 K for 18 min. (B) FTIR spectra of $Rh/Al_2O_3$ exposed to methane at 673 K for (a) 18 min, then exposed to $H_2$ at (b) 298 K for 10 min, (c) 373 K for 30 min, (d) 473 K for 10 min, and (e) 553 K for 10 min.

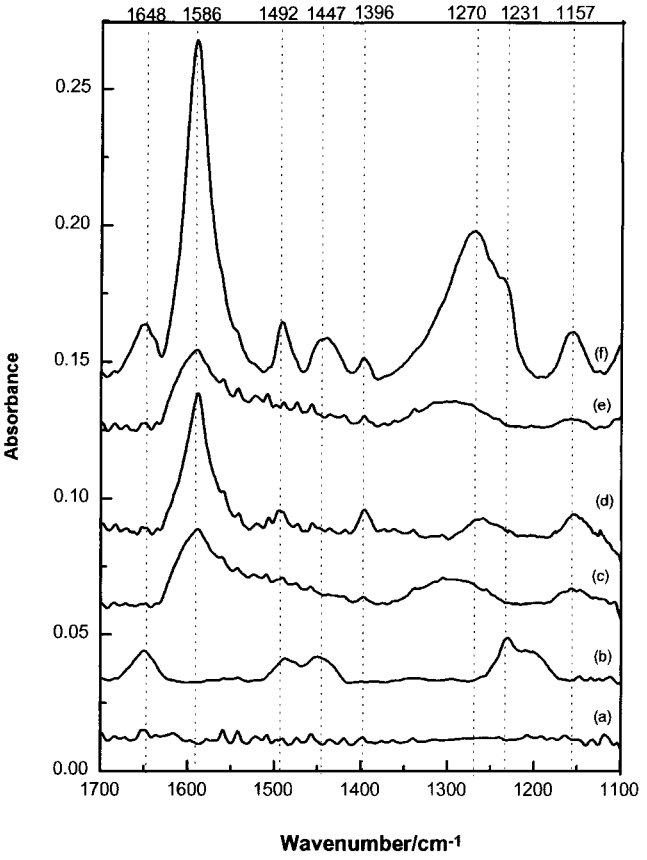


**FIG. 3.** FTIR spectra of (a) $Rh/MoAl_2O_3$ and (b) $Rh/Al_2O_3$ exposed to CO at 298 K, (c) $Rh/Mo/Al_2O_3$ and (d) $Rh/Al_2O_3$ exposed to $CH_4$ at 673 K, and (e) $Rh/MoAl_2O_3$ and (f) $Rh/Al_2O_3$ exposed to $CH_4$ at 673 K then CO at 298 K.

the spectra of samples after exposure to CO, methane, and methane and CO. Exposure to CO at 298 K lead to the appearance of bands at 1648, 1492, 1447, and 1231 $cm^{-1}$ for the $Rh/Al_2O_3$ sample (Fig. 3(b)) due to the formation of bicarbonate species (19), which were not detected for samples containing Mo (Fig. 3(a)). The $Rh/Al_2O_3$ sample heated in $CH_4$ at 673 K showed two bands centred at 1590 and 1396 $cm^{-1}$ which were due to surface formate (20). Formate at lower concentrations was also formed for the Mo-containing catalyst (Fig. 3(c)). Additionally (not shown), bands appeared at 2030 and 2038 $cm^{-1}$ for the Rh and Rh/Mo samples, respectively, indicating the generation of CO by heating the catalysts in the presence of methane alone. $Rh/Al_2O_3$ exposed to methane at 673 K followed by CO at 298 K showed bands which could be assigned to both formate and bicarbonate species in addition to a broad, intense band at 1270 $cm^{-1}$ (Fig. 3(f)). Mo-containing samples showed only weak indications for the presence of formate species (Fig. 3(e)).

Figure 4 compares IR spectra of CO adsorbed on clean $Rh/Al_2O_3$ and $Rh/Mo/Al_2O_3$ catalysts. At the lowest CO pressures used, the $Rh/Al_2O_3$ catalysts displayed bands at ca. 2100 (sh), 2068, and 2029 $cm^{-1}$ and a broad band centred at ca. 1878 $cm^{-1}$ due to bridging carbonyls (Fig. 4(a)). An increase in CO pressure had slight effects on the intensities of bands at 2068 $cm^{-1}$ due to linear bound carbonyls (21) and ca. 1878 $cm^{-1}$ due to bridge bound carbonyls but had a greater effect on the resolved 2029-$cm^{-1}$ band due to gem–dicarbonyl species (Fig. 4(b)). Further increases in pressure had little effect on band intensities for linear and bridging carbonyls and a progressively lesser effect on the intensity at 2029 $cm^{-1}$ (Fig. 4(c,d)). At the lowest CO pressures used, the $Rh/Mo/Al_2O_3$ catalysts (Fig. 4(a)) displayed bands at 2178, 2098, 2055, and 1888 $cm^{-1}$ which are assigned to adsorption at exposed Mo cation sites (22, 23), Rh gem–dicarbonyl ($\nu_{sym}$ CO), linear, and bridge bound carbonyls on Rh (21), respectively. All IR bands due to CO on Rh were significantly shifted and attenuated with respect to the Mo-free catalyst. Increasing CO pressure had little effect on the intensity of the 2055 $cm^{-1}$ band although at the highest pressure (Fig. 4B(d)) the apparent band maximum was shifted to 2063 $cm^{-1}$ and appeared as a doublet due to enhanced resolution from the 2043-$cm^{-1}$ band due to the $\nu_{asym}$ CO mode of the gem dicarbonyl. The latter species developed as a function of CO pressure as indicated by the increase in intensity at 2098 $cm^{-1}$ as did the band at 2178 $cm^{-1}$ due to adsorption at exposed cationic Mo sites. CO was most readily desorbed from $Rh(CO)_2$ or $Mo^{n+}CO$ sites rather than RhCO or $Rh_2CO$ sites by brief periods of evacuation at 298 K.

Figure 5 shows IR spectra of CO adsorbed on $CH_4$ treated (18 min contact) $Rh/Al_2O_3$ and $Rh/Mo/Al_2O_3$ catalysts. $CH_4$ treated $Rh/Al_2O_3$ catalysts in the presence of low pressures of CO exhibited bands at 2076 and 2032 $cm^{-1}$ with a broader band due to bridging carbonyls centred at ca. 1820 with a shoulder at 1899 $cm^{-1}$ (Fig. 5(a)). Increasing the pressure of CO led to increased intensities of all bands but without detectable changes in frequency (Fig. 5(b–d)). The $Rh/Mo/Al_2O_3$ catalyst after $CH_4$ treatment and exposure to CO showed a band at 2174 $cm^{-1}$ due to adsorption at exposed cationic Mo sites, a broad band centred at 2050 $cm^{-1}$, and negligible intensity in the region where bridging carbonyls on Rh may have been expected to give a band (Fig. 5(a)). All bands were of lower intensity than those for catalysts which had not been treated with $CH_4$ (Fig. 4(a)). Bands at 2174 and 2050 $cm^{-1}$ were enhanced by increases in CO pressure, but did not undergo detectable frequency shifts (Fig. 5(b–d)).

Figure 6 summarises the effects observed for both clean and $CH_4$-treated catalysts with respect to the CO pressure dependence of the intensity of the linear carbonyl band for a Mo and Mo-free rhodium catalyst. Both clean catalysts show a high proportion of the total available sites to be covered at relatively low CO pressures whereas $CH_4$-treated $Rh/Al_2O_3$ and $Rh/Mo/Al_2O_3$ catalysts show a much greater dependence on CO pressure, only achieving a high

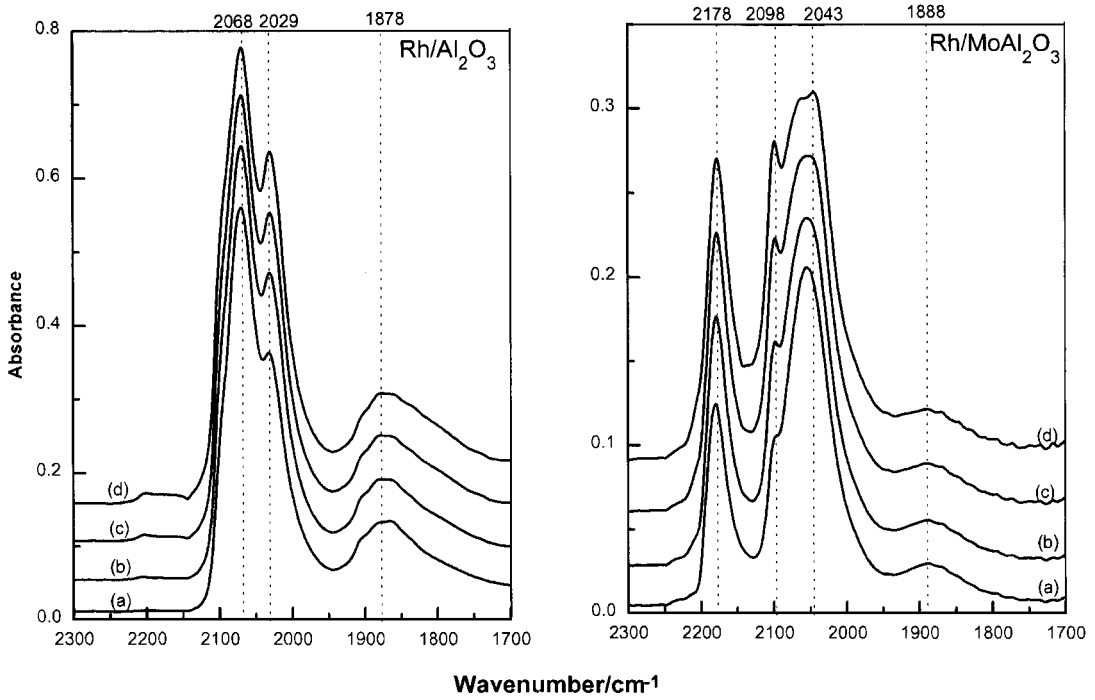


**FIG. 4.** FTIR spectra of CO adsorbed on Rh/$Al_2O_3$ and Rh/Mo/$Al_2O_3$ at pressures of (a) less than 1, (b) 1.5, (c) 5, and (d) 29 torr.

coverage for higher CO pressures (Fig. 6A). Similar observations have been made by comparing clean and $CH_4$-treated Rh–Cu catalysts (11). Evacuation readily removed CO from the $CH_4$-treated Rh/Mo/$Al_2O_3$ catalysts (Fig. 6B) but removed CO from the other samples much more slowly, which is indicative of stronger adsorption. Surprisingly, CO desorption from the coked Rh/$Al_2O_3$ surface did not follow the profile of the coked Rh/Mo/$Al_2O_3$ despite the

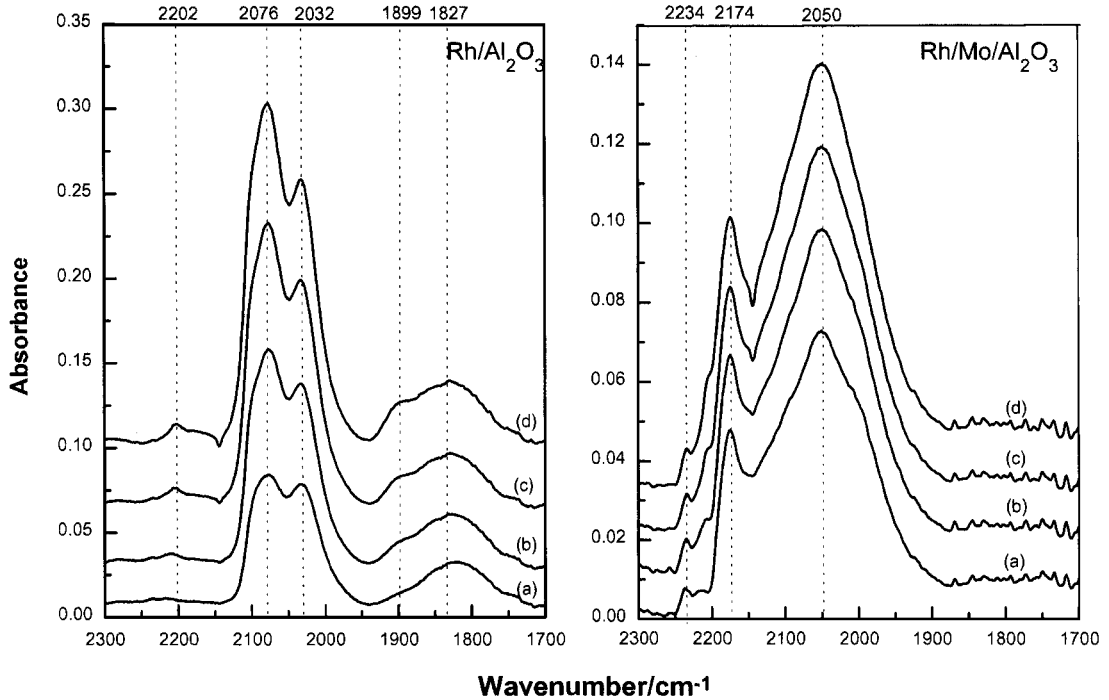


**FIG. 5.** FTIR spectra of Rh/$Al_2O_3$ and Rh/Mo/$Al_2O_3$ catalysts exposed to $CH_4$ at 673 K (18 min) followed by exposure to CO at pressures of (a) less than 1, (b) 1.5, (c) 5, and (d) 29 torr.

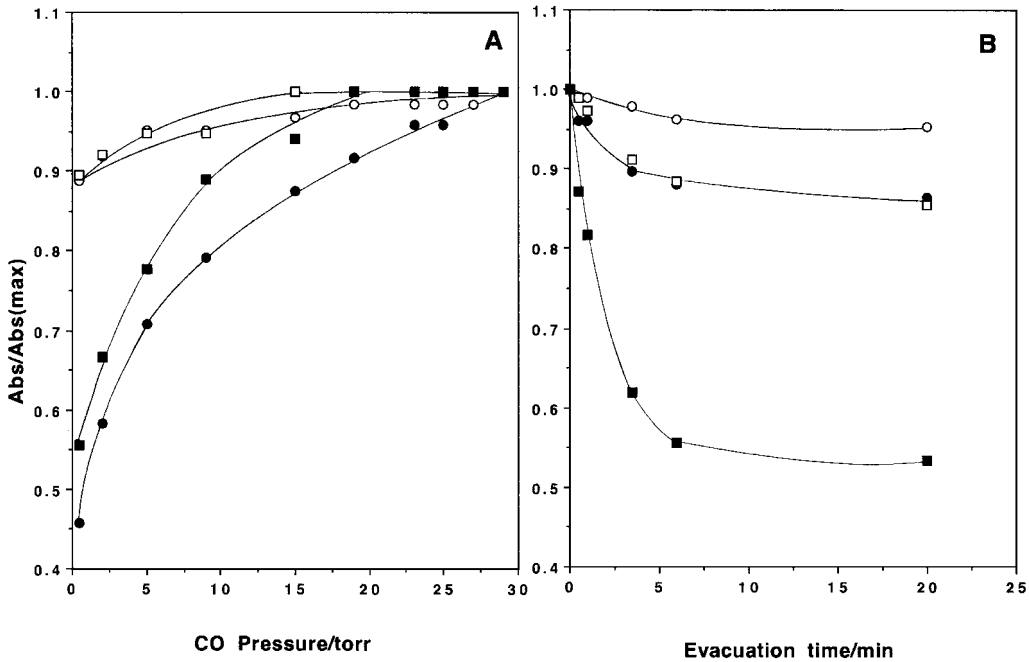


**FIG. 6.** Plots of fractional coverage (from relative absorbance due to linear carbonyl band) as a function of (A) CO pressure and (B) evacuation time at 298 K for clean (unfilled symbols) and methane treated (filled symbols) for $Rh/Al_2O_3$ (circles) and $Rh/Mo/Al_2O_3$ (squares).

similar behaviour of the two surfaces during adsorption (Fig. 6A).

Figure 7 compares IR bands due to CO adsorbed on clean surfaces, $CH_4$-treated surfaces, and after $CH_4$ treatment and subsequent hydrogenation at various temperatures for $Rh/Al_2O_3$ and $Rh/Mo/Al_2O_3$ catalysts. Hydrogenation temperatures were chosen from the reaction studies to correspond with the initial high levels of methane and the minima and maxima in methane production at ca. 373 and 473 K (Figs. 1A and 1B). Spectra of clean $Rh/Al_2O_3$ at maximum

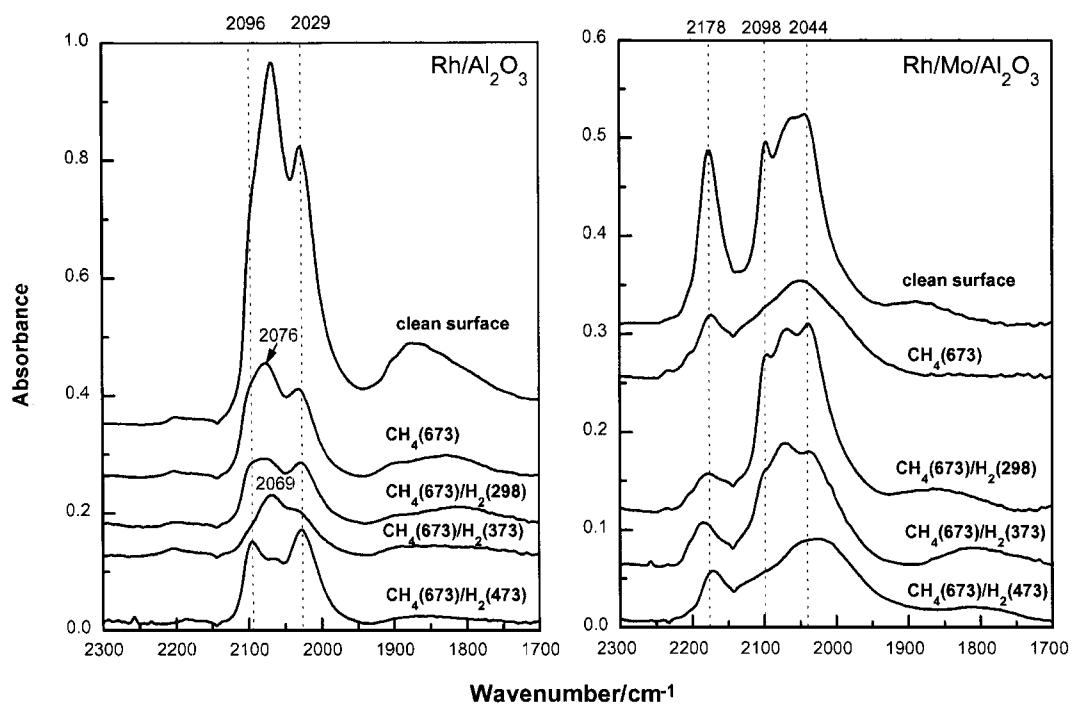


**FIG. 7.** FTIR spectra of $Rh/Al_2O_3$ and $Rh/Mo/Al_2O_3$ exposed to CO (29 torr) after reduction treatment only, or reduction and methane treatment (673 K for 18 min), or reduction and methane treatment (673 K for 18 min) followed by exposure to hydrogen at either 298, 373, or 473 K.

CO coverage showed bands at 2096 (sh) and 2029 $cm^{-1}$ due to the gem–dicarbonyl species and a more intense band at 2068 $cm^{-1}$ due to linearly bound CO. Bands due to bridging carbonyls appeared at 1904 (sh), 1878, and 1857 (sh) $cm^{-1}$ (Fig. 7a). Spectra of Rh/$Al_2O_3$ treated with $CH_4$ or $CH_4$ and subsequent hydrogen treatment failed to recover intensity at any one of these frequencies (Fig. 7(b–e)). After methane treatment alone, the sample showed bands of reduced intensity at 2096 (sh) and 2029 $cm^{-1}$ due to the gem–dicarbonyl and a band at 2077 $cm^{-1}$ due to linearly bound CO with bridging carbonyls detected at 1899 and 1828 $cm^{-1}$. A sample treatment in $CH_4$ with subsequent hydrogenation at 298 K failed to modify the spectrum in the region corresponding to bridging carbonyls but led to a general decrease of intensity of bands in the 2150–1950 $cm^{-1}$ range with the band due to linearly bound carbonyls being the most affected (Fig. 7(c)). Spectra of the methane-treated surface followed by $H_2$ treatment at 373 K showed less intense bands due to bridging and geminal carbonyls with the linearly bound species giving a band at 2069 $cm^{-1}$. Some of the intensity of the bands due to dicarbonyl species was recovered by treatment in hydrogen at 473 K (Fig. 7(e)).

Figure 7 also shows spectra of the Rh/Mo sample in the presence of the maximum pressure of CO after treating the surface in $CH_4$ alone or after $CH_4$ and subsequent hydrogen treatments. The clean surface gave carbonyl bands at 1881 (bridging), 2098 and 2044 (dicarbonyl), and 2066 $cm^{-1}$ (linear) due to adsorption on rhodium and at 2178 $cm^{-1}$ due to adsorption on the Mo component (Fig. 7(a)). Bridging carbonyls were not discernible after methane decomposition, and bands due to all other carbonyl species were weakened with the maximum due to CO on Rh appearing at 2050 $cm^{-1}$. Subsequent hydrogenation treatment at 298 K led to substantial recovery in intensity of bands due to all types of carbonyl species on the rhodium component but with minimal recovery of sites where CO was adsorbed on Mo to give the 2178 $cm^{-1}$ band (Fig. 7(c)). Bridging and linear carbonyl bands appeared at 2069 and 1844 $cm^{-1}$, respectively. $H_2$ treatments at 373 K were less successful, and less still at 473 K, at regenerating sites for CO adsorption.

## DISCUSSION

### *Location of Mo and Influence on Characteristics of Rh/$Al_2O_3$ Catalyst*

IR spectra of CO on the clean rhodium surface (Figs. 4, 7(a)) indicate three types of adsorbed carbonyls (gem–dicarbonyl, linear, and bridging) to be present, the relative contributions of which are often related to the dispersion and morphology of the metal particles present (21, 25, 26). The reduced intensities of bands due to all of these species for a Mo-containing catalyst (Fig. 4) in addition to the reduced hydrogen uptake (Table 1) confirm previous results for Rh–Mo catalysts (18, 22, 27, 28) that the addition of molybdenum decreases the number of exposed rhodium atoms, although this does not necessarily infer (25) a loss in Rh dispersion. Previous IR results have been interpreted (22) as a migration of molybdenum over the surface of Rh particles to form a phase which does not chemisorb CO. The appearance of the band at 2178 $cm^{-1}$ (Fig. 4) which is not detected for Rh in the absence of Mo (Fig. 4) indicates that at least a fraction of the exposed Mo ions do chemisorb CO. Bands in this region have been assigned (22, 23, 28) to CO adsorbed on $Mo^{4+}$, $Mo^{3+}$, and $Mo^{2+}$ sites. The latter assignment was made on the basis of adsorption on well-defined sites generated by the use of allyl precursors (28) and agrees with XPS results (18) of similar catalysts in which $Mo^{6+}$ and $Mo^{2+}$ were the predominant surface species after similar reduction treatments. These ions probably exist as isolated species (28) on the alumina support and as such do not directly influence the behaviour of the active Rh component. The absence of bicarbonate species on the alumina surface (Fig. 3) following exposure to CO is consistent with the distribution of Mo species over the support surface. Sites responsible for the absorption band at 2178 $cm^{-1}$ could be eliminated by performing a reduction–oxidation–reduction cycle (29) which generated $Mo^0$ sites which were present in a Rh–Mo alloy phase (18). Although Mo atoms in the surface of such phases may not adsorb CO (22), their presence would be expected to modify the adsorption behaviour of neighbouring Rh atoms.

Dilution of the rhodium surface (22) by Mo atoms may be expected to modify the relative number of bridging sites to a greater extent than sites where CO is adsorbed on top. This is confirmed by analysis of the band intensities due to the respective species for the two samples (Fig. 4) where the intensity of the linear band is 5.3 times lower in the presence of Mo but 13.5 times less for bridging sites. The exact preference of these Mo atoms for a particular type of site is not readily derived from band positions of bridging carbonyls. A single broad maximum existed for Rh in the presence of Mo while in its absence the band due to bridging carbonyls could be readily deconvoluted into three maxima at 1904, 1878, and 1859 $cm^{-1}$ (Fig. 4). At full coverage, vibrational frequencies of 1940 and 1850 $cm^{-1}$ are obtained for bridging carbonyls on Rh (100) and Rh (111), respectively (30–32), while step atoms in the Rh (331) surface may adsorb CO in the bridging mode with a vibrational frequency of 1930 $cm^{-1}$ (33). However, as a shift from 1880 to 1940 $cm^{-1}$ mainly due to dipole coupling effects accompanies an increase in CO coverage of the Rh (100) face (30), and the effect of Mo diluting the Rh surface would be a reduction in coupling interactions due to a decrease in the relative number of neighbouring carbonyls on rhodium, assignment of the remaining band due to bridging carbonyls on a specific face, implying a blocking effect of Mo atoms on the others, would be tenuous. Similarly, reduced intensity and a lower frequency (2063 compared with 2068 $cm^{-1}$) of linear rhodium

carbonyls in the presence of Mo could be readily interpreted in terms of surface dilution reducing the average number of coupling interactions experienced by each carbonyl species. The shift to lower wavenumbers for the linear Rh carbonyl band in the presence of Mo is the opposite to the effect previously reported for $RhMo/Al_2O_3$ (22, 24) and to the shift observed when these catalysts were treated in a reduction–oxidation–reduction cycle (29). One explanation is that the latter treatment (29) and preparation procedures used elsewhere (22, 24) generate mainly bimetallic Rh–Mo phases (34, 35), while the procedure adopted here produces Rh crystallites which are partially coated with Mo atoms. In studies where the Rh–carbonyl exhibits a blue shift in the presence of Mo (22, 24, 29), the band due to CO on $Mo^{2+}$ (28) appears at most as a very weak feature. The detection here of a strong band at 2178 $cm^{-1}$ indicates that a significant fraction of the Mo exists as isolated $Mo^{2+}$ (28) due to spreading (23) and strong interaction with the alumina support. Treatments and preparations that avoid or overcome this strong interaction favour the Rh–Mo interaction and the formation (34, 35) of Rh–Mo alloy phases.

In addition to the band shift of linear carbonyls induced by the presence of molybdenum, the band due to the asymmetric stretching mode of the rhodium gem–dicarbonyl (21, 24, 25) appeared at 2043 $cm^{-1}$ in the presence of Mo (Figs. 4 and 7) but at ca. 2030 $cm^{-1}$ in its absence (Figs. 4, 5, and 7). This detail has been observed in previous studies and attributed (27, 36) to the presence of an additional type of rhodium–dicarbonyl site which is in a more oxidised state due to the presence of Mo. However, studies comparing various supports have shown the gem–dicarbonyl species to be sensitive to the metal–support interaction with the stretching parameter, $k$ (CO), showing a large degree of dependence on the support used (37), and so modification of the alumina by addition of 10% $MoO_3$ is not unexpected. No diffraction pattern for crystalline molybdenum species was detected and CO adsorption at 298 K (Fig. 3(a)), unlike the result for $Rh/Al_2O_3$ alone (Fig. 3(b)), did not lead to the formation of bicarbonate species indicating that the molybdena was present mainly as a dispersed phase over the alumina support.

*Methane Decomposition*

Decomposition of methane at 673 K over the rhodium containing catalysts led to the appearance of IR bands at 2030 and 2038 $cm^{-1}$ due to adsorbed CO indicating that carbon monoxide was generated during the reaction. Spectra of the low frequency region (Fig. 3) show the presence of formate species on the alumina support which may also be generated by a reaction between CO and hydroxyl groups on the support (20). The detection of formate species via methane reaction at 673 K (Fig. 3(c,d)) as opposed to bicarbonate species from CO at 298 K (Fig. 3(a,b)) is consistent with the different thermal stability of these species on alumina where increasing the temperature leads to the generation of formate species with the concurrent elimination of bicarbonate (38). The formation of CO from methane over supported rhodium catalysts has been observed (8) and attributed to a reforming reaction between the carbonaceous deposits generated by $CH_4$ decomposition and hydroxyl groups of the oxide support. However, loss of OH groups during $CH_4$ conversion (39) does not necessarily implicate (8) these species in the reaction to produce CO as the generation of formate species from CO (20) would also account for the consumption of hydroxyls.

Both hydrogen chemisorption (Table 1) and IR of adsorbed CO (Fig. 7) indicate a fraction of the metal surface to be covered following reaction in methane at 673 K. The hydrogen chemisorption measurements at 298 K most likely do not, however, give a quantitative indication of the fraction of sites covered by residue as results in Fig. 1 indicate that reaction between the residue and hydrogen to produce mainly $CH_4$ may occur at these temperatures making the volumetric measurements highly dependent on the C : H ratio of the residue. Partially carbon covered metal surfaces have been reported to chemisorb close to one monolayer of hydrogen, due to an additional hydrogen uptake associated with the $\beta$-form of carbon (40). IR of CO (Fig. 7) at least qualitatively supports the chemisorption results (Table 1) in that a fraction of the metal surface remained unavailable for adsorption following reaction with methane at 673 K.

Comparing the overall band envelope for CO on the clean and methane-treated Rh and Rh/Mo surfaces (Fig. 7) suggests that all types of Rh sites are affected to a similar extent for $Rh/Al_2O_3$ (Fig. 7(a,b)), while the $Mo^{2+}$ and rhodium bridging and dicarbonyl sites are influenced to a greater extent than the sites for linear adsorption of CO on the $Rh/Mo/Al_2O_3$ surface.

The presence of carbonaceous residue affects the subsequent adsorption of CO (Fig. 6), a higher pressure being required to obtain an equivalent fractional coverage than the corresponding pressure for a clean surface. An explanation invoking diffusion limitations on the rate of CO reaching the metal surface in the presence of the carbonaceous residue is not tenable because experiments conducted leaving extended intervals between exposure to CO and recording of the spectrum produced identical results. Should the need for higher CO pressures to reach equivalent fractional coverage be a result of weakened adsorption in the presence of coke (42), this should be manifested in the ease of desorption and in the frequencies of the adsorbed CO bands. Spectra obtained by degassing between 30 s and 20 min indicate (Fig. 6B) that only the coked $Rh/Mo/Al_2O_3$ surface readily desorbed CO. Differences in the desorption behaviour of CO from the two coked surfaces despite the similarities in the adsorption behaviour as a function of

pressure, giving rise to hysteresis in the CO adsorption isotherm for coked $Rh/Al_2O_3$, would suggest that modifications occurred to the surface carbon layer during the adsorption process. The presence of coke results in a blue shift of the linear carbonyl band for Rh (2068 to 2076 $cm^{-1}$ at full coverage) but a red shift (2063 to 2050 $cm^{-1}$ at full coverage) for RhMo. Clearly the band frequencies will be strongly dependent on whether clustering of the adsorbed carbonaceous material occurs and the exact nature (C : H ratio) of the residue, both of which may be influenced by the presence of Mo. A further possibility, supported by STM results (41) for Pt (111) and IR results for Rh–Cu catalysts (11) is that adsorption of CO induces a reorganisation of the surface carbonaceous deposits, with an increase in CO pressures leading to the creation of additional adsorption sites as restructuring occurs. This restructuring of the carbon residue apparently occurs to a greater extent for $Rh/Al_2O_3$ than for $Rh/Mo/Al_2O_3$ judging from the different CO desorption profiles obtained (Fig. 6B). This restructuring in the presence of CO may be related to the process which at higher temperatures, leads to dislodging of the adspecies generated by methane adsorption on $Pt/SiO_2$ and the release of hydrocarbon product (43).

The nature of the species responsible for blockage of metal sites may be deduced from IR spectra in the CH stretching region (Fig. 2). The most intense maxima, which appear at 3045 $cm^{-1}$ for both Mo-containing and Mo-free $Rh/Al_2O_3$ catalysts, do not correspond with vibrational frequencies for adsorbed $CH_3$ on rhodium (44). This single maximum without corresponding features due to other stretching modes of the same species indicates a C–H group. The inability to record spectra below 1000 $cm^{-1}$ where the two deformation modes may or may not be detected in accordance with the surface selection rule, prevents differentiation between a C–H species bound perpendicular to the metal surface and a $C_x$–H-type species. The latter, where $x$ is generally 2, is identified by a band at ca. 3040 $cm^{-1}$ in HREELS spectra of $C_2$, $C_3$, $C_4$ hydrocarbons and benzene adsorbed on Rh (111) upon heating between 450–800 K (45, 46).

The growth in the band at 3045 $cm^{-1}$ as a function of time, even after 60 min contact, shows the progressive increase in carbonaceous material deposited. Accepting the possible error in the relative number of available sites after coking as measured by volumetric $H_2$ adsorption, the Mo-containing sample shows a greater percentage loss of sites (63% compared with 40%) which is at least qualitatively in line with the relative intensity of the band at 3045 $cm^{-1}$ indicating that the species responsible is at least in part located on the metal surface. Calculated values of C/metal atom ratios for $Rh/Al_2O_3$ catalysts show the amount of deposited coke to be greater than the number of metal sites (8) suggesting that at least part of this coke is located on the support surface. The loss in intensity of the carbonyl band at 2178 $cm^{-1}$ after coking further supports a spreading of the coke over an area more extensive than just the metal surface.

*Hydrogenation of Hydrocarbonaceous Deposits*

Further indication that the C–H species giving the band at 3045 $cm^{-1}$ is at least in part located on the metal surface is given by the loss of intensity at this frequency (Fig. 2B(b)) and the regeneration of sites available for chemisorption of CO (Fig. 7) when the samples were exposed to hydrogen at 298 K. Recovery of sites as determined by the intensity of IR bands due to CO adsorbed on RhMo following hydrogenation treatments at different temperatures (Fig. 7) shows qualitative agreement with the temperatures at which gas-phase product is generated (Fig. 1). The fraction of sites which can be recovered for Rh–Mo is progressively diminished with increasing hydrogenation temperature, consistent with the general form of the plots in Fig. 1. In the case of Rh alone, recovery of appreciable sites for CO adsorption (Fig. 7(e)) occurs only after heating in $H_2$ at 473 K, consistent with the detection of methane as a gas-phase product by GC (Fig. 1A) and in IR spectra recorded following similar treatment (Fig. 2B(d)). The relative proportion of each type of adsorption site on rhodium (bridging, linear, and geminal), which was recovered as a function of hydrogenation temperature for the Mo-containing catalyst, was very similar, preventing conclusions being made regarding particular location of deposits. However, the 2178-$cm^{-1}$ band due to adsorption at exposed $Mo^{2+}$ sites which was attenuated by coking in methane at 673 K (Fig. 7(a,b)) could not be recovered regardless of the hydrogenation temperature. Studies using supported and unsupported Mo compounds indicate that interactions with methane at temperatures around 973 K lead to the formation of $Mo_2C$ which is considered the active site for formation of $CH_2$ and $CH_3$ fragments (14, 16). These carbides may be destroyed by reaction with air or $CO_2$ (16). Although the presence of Rh in RhMo catalysts has been shown to enhance $Mo^0$ formation at low temperatures (18, 34), which would facilitate carbide formation, the loss of intensity of the 2178-$cm^{-1}$ band after exposure to methane at 673 K is probably not due to formation of bulk Mo carbide type species (14, 16) but to a surface carbonaceous species which is not readily hydrogenated by thermal treatment in hydrogen at up to 473 K (Fig. 7B).

A comparison of spectra for CO adsorbed on methane-treated RhMo surfaces followed by hydrogen indicates that an almost complete recovery of Rh sites is possible (hydrogenation at 298 K) whereas a significant proportion of coked Rh sites remains inaccessible to CO after $H_2$ treatment in the temperature range 298–473 K for the Mo-free Rh catalysts (Fig. 7). Three types of surface carbonaceous species ($\alpha$, $\beta$, and $\gamma$) are thought to form on metal surfaces exposed to $CH_4$ with interconversion between these

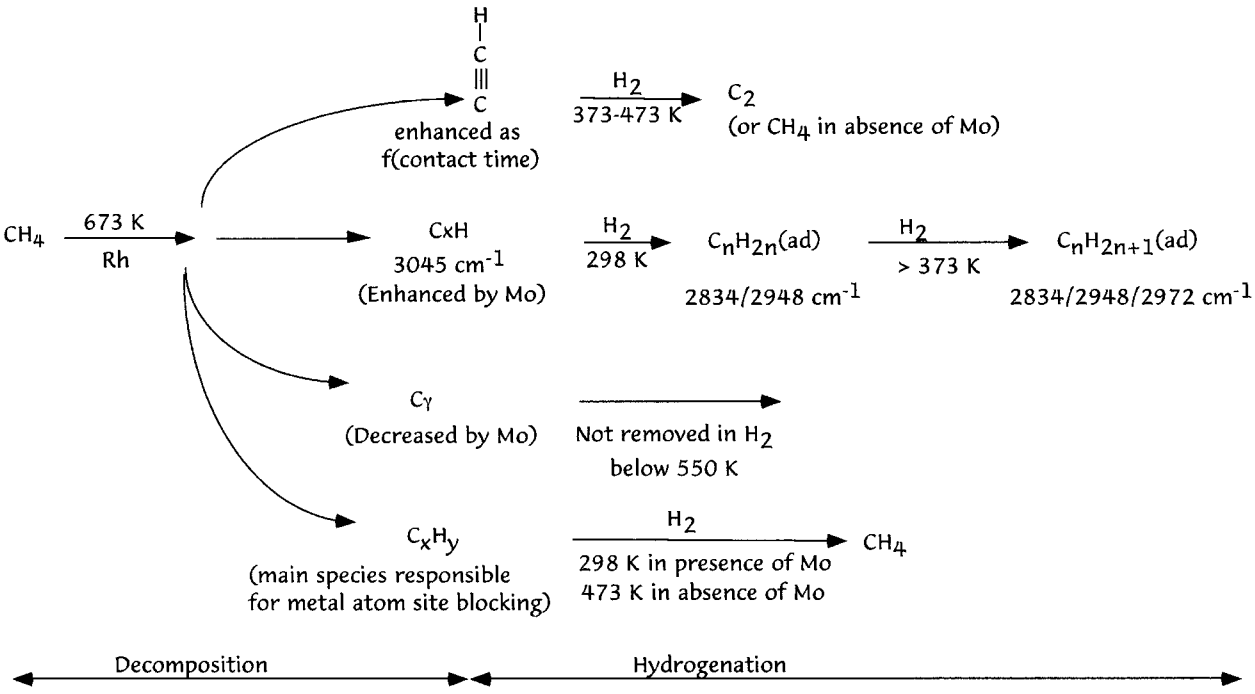


**FIG. 8.** Schematic representation of the relationship between species formed during the decomposition of methane and subsequent hydrogenation over $Rh/Al_2O_3$ and $Rh/Mo/Al_2O_3$ catalysts.

species eventually leading to the formation of the graphitic-like $C_\gamma$ phase which is only hydrogenated at higher (ca. 673 K) temperatures (6). For a Mo-free Rh catalyst, methane was only detected at hydrogenation temperatures of 473 K (Figs. 1A and 2B(d,e)). A plausible explanation for results here would be that dilution of the Rh surface by the presence of Mo hinders the ageing of the carbonaceous deposits, allowing these to be hydrogenated at lower temperatures. This hindrance of the interconversion of the various carbonaceous species in the presence of Mo may also be linked to the reduced mobility of the carbonaceous deposits in the presence of CO, which resulted in the more pronounced restructuring phenomena detected for Mo-free Rh catalysts.

Although greatest recovery of sites for $Rh/Al_2O_3$ occurs following hydrogen treatment at 473 K (Fig. 7e) with little recovery at 298 K (Fig. 7c), the latter treatment results in the most significant loss in intensity of the 3045 $cm^{-1}$ band (Fig. 2B(a,b)) showing other carbonaceous species to be primarily responsible for site blocking. The $C_xH$ species giving the 3045-$cm^{-1}$ band does not appear to be a direct precursor of methane, as the latter was detected only after heating of the $Rh/Al_2O_3$ in $H_2$ at 473 K (Fig. 2B(d)) although ca. 70% of the $C_xH$ species underwent reaction at 298 K. Loss of the 3045-$cm^{-1}$ band intensity, however, does correlate with the appearance of the 2948/2834 $cm^{-1}$ pair which can be assigned to the asymmetric and symmetric stretching vibrations of $CH_2$ groups. The appearance of a third feature at 2972 $cm^{-1}$ due to the asymmetric stretching vibrations of $CH_3$ groups occurs at a higher hydrogenation temperature when increased levels of $CH_2$ groups are detected, making it difficult to conclude whether long chain alkyl groups (with terminal methyl groups) are being produced or whether $CH_2$ to $CH_3$ hydrogenation of smaller fragments is being detected. The absence of correlation with gas phase product detection would favour the former assignment.

Bands which remain to be assigned following methane decomposition are observed at 3382, 3336, and 3290 $cm^{-1}$ (Fig. 2A). These frequencies for carbon–hydrogen stretching frequencies are indicative of *sp* hybridisation as in acetylene, suggesting C≡C–H type species. Although a link with gas-phase products would be extremely tenuous, their disappearance from the spectra of the sample in hydrogen between 373 and 473 K (Fig. 2B(c,d)) coincides with the temperature range of the second maxima where products are evolved (Fig. 1), including the formation of $C_2$ hydrocarbons (Fig. 1C). If the assignment and the link are correct, then this finding is of considerable significance given the arguments as to whether C–C bond formation occurs during the methane decomposition step or the subsequent hydrogenation stage (43, 47). The overall, two-stage decomposition and hydrogenation scheme is represented in Fig. 8.

## CONCLUSIONS

Methane decomposes over $Rh/Mo/Al_2O_3$ catalysts at 673 K to produce $C_xH$ species and other amorphous carbon species with the latter primarily responsible for metal

site blocking. Co-adsorption studies with CO indicate that the carbonaceous residues are mobile and may undergo restructuring. The presence of Mo enhances the amount of decomposition product formed for $Rh/Al_2O_3$. Recovery of metal sites may be achieved by hydrogenation of the carbonaceous residues at 298–473 K to produce mainly methane and some $C_2$ hydrocarbons. Mo in the $Rh/Al_2O_3$ catalyst enhances the extent to which coke removal takes place in hydrogen at low temperatures, possibly by restricting the mobility and thus by ageing of the residues. Hydrogenation of $C_xH$ species (3045 $cm^{-1}$) releases few metal sites and leads to the formation of long chain alkyl groups which are retained by the catalyst.

## ACKNOWLEDGMENTS

We thank the Royal Society (London) for a University Research Fellowship (J.A.A.), the University of Dundee for a Postgraduate Studentship (Z.W.), and Johnson Matthey for the loan of Rh $(NO_3)_3$.

## REFERENCES

1. Parkyns, N. D., *Chem. Britain*, 841 (1991).
2. Rostrup-Nielson, J. R., *in* "Catalysis, Science and Technology" (J. R. Anderson and M. Boudart, Eds.), Vol. 5. Springer-Verlag, Berlin, 1984.
3. Peña, M. A., Gómez, J. P., and Fierro, J. L. G., *Appl. Catal.* **144**, 7 (1996).
4. Baerns, M., van der Wiele, K., and Ross, J. R. H., *Catal. Today* **4**, 471 (1989).
5. Brown, J. J., and Parkyns, N. D., *Catal. Today* **8**, 305 (1991).
6. Guczi, L., van Santen, R. A., and Sarma, K. V., *Catal. Rev. Sci. Eng.* **38**, 249 (1996).
7. Solymosi, F., Erdöhelyi, A., and Cserényi, J., *Catal. Letts.* **16**, 399 (1992).
8. Ferreira-Aparicio, P., Rodriguez-Ramos, I., and Guerrero-Ruiz, A., *Appl. Catal.* **148**, 343 (1997).
9. Pareja, P., Molina, S., Amariglio, A., and Amariglio, H., *Appl. Catal.* **168**, 289 (1998).
10. Solymosi, F., and Cserényi, J., *Catal. Letts.* **34**, 343 (1995).
11. Anderson, J. A., Rochester, C. H., and Wang, Z., *J. Molec. Catal.* **139**, 285 (1999).
12. Wong, S.-T., Xu, Y., Liu, W., Wang, L., and Guo, X., *Appl. Catal.* **136**, 7 (1996).
13. Pierella, L. B., Wang, L., and Anunziata, O. A., *React. Kinet. Catal. Letts.* **60**, 101 (1997).
14. Solymosi, F., Cserényi, J., Szoke, A., Bánsági, T., and Oszkó, A., *J. Catal.* **165**, 150 (1997).
15. Liu, S., Dong, Q., Ohnishi, R., and Ichikawa, M., *Chem. Commun.* 1455 (1997).
16. Wang, D., Lunsford, J. H., and Rosynek, M. P., *Topics in Catal.* **3**, 289 (1996).
17. Chen, L., Lin, L., Xu, Z., Zhang, T., and Li, X., *Catal. Lett.* **39**, 169 (1996).
18. Anderson, J. A., Guerrero-Ruiz, A., and Fierro, J. L. G., *Topics in Catal.* **1**, 123 (1994).
19. Parkyns, N. D., *J. Chem. Soc. (A)*, 1910 (1967).
20. Gopal, P. G., Schneider, R. L., and Watters, K. L., *J. Catal.* **105**, 366 (1987).
21. Anderson, J. A., and Rochester, C. H., *J. Chem. Soc. Faraday Trans.* **87**, 1479 (1991).
22. DeCanio, E. C., and Storm, D. A., *J. Catal.* **132**, 375 (1991).
23. Zaki, M. I., Vielhaber, B., and Knozinger, H., *J. Phys. Chem.* **90**, 3176 (1986).
24. Yang, A. C., and Garland, C. W., *J. Phys. Chem.* **61**, 1504 (1957).
25. Rice, C. A., Worley, S. D., Curtis, C. W., Guin, J. A., and Tarrer, A. R., *J. Chem. Phys.* **74**, 6487 (1981).
26. Storm, D. A., Mertens, F. P., Cataldo, M. C., and DeCanio, E. C., *J. Catal.* **141**, 478 (1993).
27. Hecker, W. C., Wardinsky, M. D., Clemmer, P. C., and Breneman, R. B., *in* "Proc. 9th Int. Cong on Catal" (M. J. Philips and M. Ternan Eds.), p. 1106. Chem. Inst. Canada, Ontario, 1988.
28. Brito, J. L., and Griffe, B., *Catal. Lett.* **50**, 169 (1998).
29. Anderson, J. A., Rochester, C. H., and Wang, Z., unpublished results.
30. Leung, L.-W. H., He, J.-W., and Goodman, D. W., *J. Chem. Phys.* **93**, 8328 (1990).
31. de Jong, A. M., and Niemantsverdriet, *J. Chem. Phys.* **101**, 10126 (1994).
32. Root, T. W., Fisher, G. B., and Schmidt, L. D., *J. Chem. Phys.* **85**, 4887 (1986).
33. Dubois, L. H., Hansma, P. K., and Somorjai, G. A., *J. Catal.* **65**, 318 (1980).
34. Kunimori, K., Wakasugi, T., Yamakawa, F., Oyanagi, H., Nakamura, J., and Uchijima, T., *Catal. Lett.* **9**, 331 (1991).
35. Lamber, R., Jaeger, N. I., Trunschke, A., and Meissner, H., *Catal. Lett.* **11**, 1 (1991).
36. Wardinsky, M. D., and Hecker, W. C., *J. Phys. Chem.* **92**, 2602 (1988).
37. Miessner, H., Gutschick, D., Ewald, H., and Müller, H., *J. Molec. Catal.* **36**, 359 (1986).
38. Amenomiya, Y., *J. Catal.* **57**, 64 (1979).
39. Buyevskaya, O. V., Wolf, D., and Baerns, M., *Catal. Lett.* **29**, 249 (1994).
40. Winslow, P., and Bell, A. T., *J. Catal.* **91**, 142 (1985).
41. McIntyre, B. J., Salmeron, M., and Somorjai, G. A., *J. Catal.* **164**, 184 (1996).
42. Abon, M., Billy, J., Bertolini, J. C., and Tardy, B., *Surf. Sci.* **167**, 1 (1986).
43. Amariglio, H., Belgued, M., Paréja, P., and Amariglio, A., *Catal. Lett.* **31**, 19 (1995).
44. Solymosi, F., *Catal. Today* **28**, 193 (1996).
45. Dubois, L. H., Castner, D. G., and Somorjai, G. A., *J. Chem. Phys.* **72**, 5234 (1980).
46. Bent, B. E., Mate, C. M., Crowell, J. E., Koel, B. E., and Somorjai, G. A., *J. Phys. Chem.* **91**, 1493 (1987).
47. Amariglio, A., Paréja, P., and Amariglio, H., *J. Catal.* **166**, 121 (1997).